Langmuir

ARTICLE

pubs.acs.org/Langmuir

Branched Networks by Directed Assembly of Shape Anisotropic Magnetic Particles

Priyadarshi Panda, Ki Wan Bong, T. Alan Hatton, and Patrick S. Doyle*

Department of Chemical Engineering, Massachusetts Institute of Technology, Cambridge, Massachusetts 02139, United States

Supporting Information

ABSTRACT: The directed assembly of shape anisotropic magnetic particles into targeted macrostructures requires judicious particle design. We present a framework to understand the self-assembly of magnetic non-Brownian H-shaped particles and the formation of branched networks under an applied magnetic field. A finite element integration (FEI) method is developed to identify the preferred particle orientation (relative to the applied field) at different values of the geometric parameters defining H shapes, and used to construct a phase diagram to generalize the results. Theoretical predictions are validated by comparing with experiments performed using magnetic hydrogels synthesized using stop-flow lithography (SFL). We demonstrate the ability of H-shaped particles to form chains parallel to the field that can thicken in a direction orthogonal to the field, and in some cases with branching. The assembly of a suspension containing H-shaped particles, or rods, or a combination of both, is reported.

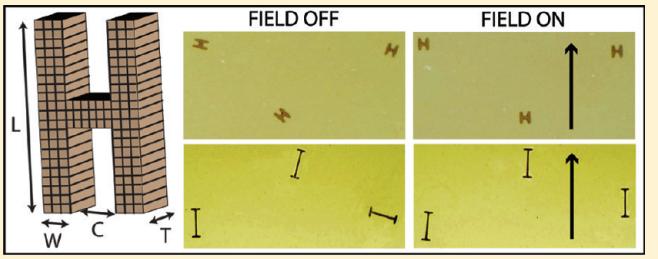

1. INTRODUCTION

The macroscopic properties of electrorheological (ER) and magnetorheological (MR) fluids depend on the microstructure formed on applying electric or magnetic fields.[1−3] Since colloids used in these responsive fluids have primarily been spherical in shape due to ease of synthesis and ready availability, the structures formed by ER and MR fluids composed of spherical field-responsive colloids under different conditions have been the topic of many studies (see ref 4 for a recent review). Field-responsive shape-anisotropic particles, specifically rod-shaped particles, have been shown to form stronger ER[5−9] and MR[10−14] fluids than do spherical particles, and also provide better stability against sedimentation and easy redispersion.[9−12,14] Hence, the focus of many recent studies has been to tune the properties of ER and MR fluids by designing anisotropic particles.[4] The study of rotation and assembly of anisotropic field-responsive particles and the structures they form is nascent;[15] however. Studies have been reported wherein electric/magnetic fields have been used to assemble "shape",[16−22] "chemically",[20,23−27] and "both shape and chemically"[22] anisotropic field-responsive particles. The studies with shape anisotropic particles have considered rods,[13,14,28,29] ellipsoids,[18,30] peanuts,[17,31] cubes,[16] hexnuts and boomerangs,[19] chiral plates,[32] toroids,[20] blocks,[21] and triangles[22] wherein the particles form either chains or dense clusters under an applied magnetic field.

Both spherical and anisotropic (rod-shaped) particles used in MR fluids form chains under an applied magnetic field at low concentrations. Widening of these chains in a direction orthogonal to the applied field (column formation) occurs at higher concentrations[14] and has been implicated in the enhanced ER and MR performance noted for whisker-shaped[8] and rod-shaped[13] particles, respectively. A simple shape that can potentially promote such chain widening, and formation of branched networks at low particle concentrations is that of an H (Figure 1). When mixed with MR spheres, one might envision that each vertical arm of the H could be integrated into separate linear chains, with the horizontal arm of the H acting to bridge the chains. Thus, more broadly, H shapes can be visualized as microparticle analogues to cross-linkers in polymer chemistry. They could be used to vary network topology and the resulting mechanics in MR suspensions.

Two distinct motions occur during the assembly of anisotropic field-responsive particles: rotation and translation.[33] These motions have associated characteristic time scales: a rotational time scale given by the time required for a single isolated anisotropic particle to rotate into an equilibrium orientation, and a translational time scale for the center of mass movement driven by particle−particle interactions and given by the time required for particles to form assembled structures with neighboring particles. Hence, a clear understanding of the equilibrium orientation attained by anisotropic particles is essential for further studies on their assembly.

There has been a longstanding interest in orienting anisotropic field-responsive biological entities. The equilibrium orientation of cells has been studied with a focus on their directed motion[34,35] or as a means to create engineered heart tissue with preferential orientation.[36] Furthermore, living species such as magnetotactic bacteria are known to swim along magnetic field

Received: June 19, 2011
Revised: September 19, 2011
Published: September 20, 2011

lines[37,38] by arranging intracellular organelles containing magnetic crystals called magnetosomes into chains which align in the direction of the field lines.[38] The living entities considered in the aforementioned studies can be modeled as ellipsoidal or rodlike particles. As opposed to rods or ellipsoids which orient along their primary axis under a uniform magnetic field,[28,30,33,35,36,38,39] the equilibrium orientation of more complicated shapes is nontrivial and depends on the geometric parameters defining the shape.

In this work, we study the dependence of the equilibrium orientation of non-Brownian H-shaped magnetic hydrogels on geometric parameters using both numerical techniques and experiments. We further simplify the system by considering particles which are confined to rotate in-plane. Experimentally, a quasi-2D suspension is realized by fabricating large dense particles which readily sediment to the bottom of the observation chamber. Applying the magnetic field tangent to the focal plane of the imaging optics allows us to monitor accurately particle rotation. We begin by describing the finite element integration (FEI) technique, followed by presenting the FEI predictions in the form of a phase diagram through which we show that the rotation of H-shaped particles can be tuned by geometric parameters in a nontrivial manner. The predictions are then validated by experiments using magnetic hydrogels synthesized using stop-flow lithography (SFL).[40]

We use the results obtained from the rotation study to design experiments to test the ability of H-shaped particles to assemble into wide (orthogonal to the field) chains. We performed assembly experiments using a mixture of rods and H-shaped particles at a low total surface coverage, and investigated the effect of varying the fraction of H-shaped particles on orthogonal chain growth. Finally, we show that chain growth orthogonal to the field can occur via two modes, branching and meandering, and quantify the degree of branching using suitable statistical measures.

2. THEORY AND MODELING

In this study, we use non-Brownian 2D extruded (e.g., rectangular cross section) H-shaped magnetic hydrogels with encapsulated nanometer sized beads (Figure 1). The H-shaped particles comprise two vertical rods of length and breadth L and W, respectively, connected to each other by a horizontal rod of length and breadth C and W, respectively. At the nanoparticle loadings used in the experiments, the mean nanoparticle separation is much smaller than the microparticle feature sizes. Hence, we can assume a homogeneous distribution of beads in our H-shaped hydrogels. We simplify our system further by modeling our 2D extruded particles as quasi-2D particles of thickness T, where T is small compared to the other geometric parameters of the H shape (Figure 1). It can be shown that the orientation with minimum energy for a quasi-2D particle would be the same as that for our 2D extruded particles (see the Supporting Information). We divide the H-shaped magnetic hydrogel into cuboidal meshes of size s along both the x and y axis and T along the z axis, having a constant magnetization M. We treat the mesh elements as point dipoles placed at the centers of the meshes (Figure 1B). The energy of interaction between mesh elements (1,2) is then given by

$$U_{12} = \frac{\mu_o}{4\pi} \frac{\mathbf{m}_1 \cdot \mathbf{m}_2 - 3(\hat{\mathbf{r}}_{12} \cdot \mathbf{m}_1)(\hat{\mathbf{r}}_{12} \cdot \mathbf{m}_2)}{{r_{12}}^3} \quad (1)$$

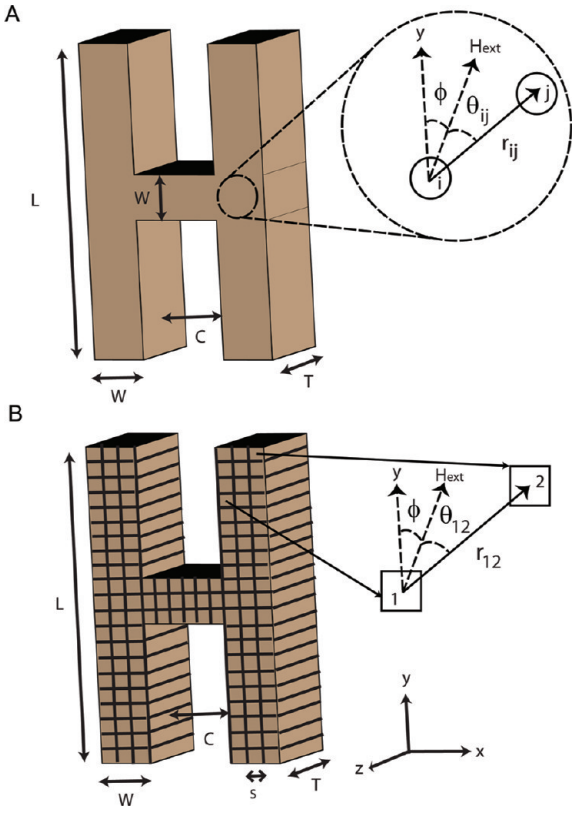

Figure 1. (A) Schematic for a 2D extruded H-shaped particle. The particles are made up of a homogeneous distribution of magnetic beads as represented by i and j. The angle made by the vector joining the center of the beads i and j with the magnetic field vector is given by θ_{ij}. (B) H shapes are divided into cuboidal meshes of size s along both the x and y axis and T along the z axis for evaluating the energy using FEI. FEI involves summing the interaction energies between all the mesh elements. The angle (orientation) made by the magnetic field with the y axis is denoted by ϕ, where ϕ can take values from 0° to 90°.

where μ_o is the permeability of free space, $\mathbf{r}_{12}$ is the vector connecting the centers of mesh elements 1 and 2, $\mathbf{m}_1$ and $\mathbf{m}_2$ are the dipole moments of mesh elements 1 and 2, respectively, and $\hat{\mathbf{r}}_{12}$ is the unit vector in the $\mathbf{r}_{12}$ direction. The magnitude of the dipole moment of each mesh element is given by

$$m = VM \quad (2)$$

where M is the volumetric magnetization of the hydrogel and V is the volume of the mesh element. The magnetization of the hydrogel (M) depends on the weight fraction of beads encapsulated in the hydrogel and can be determined experimentally. The saturation magnetization of the hydrogel is equal to the product of the weight fraction of beads encapsulated in the hydrogel and the saturation magnetization of the beads. The direction of the dipole moment of a mesh element is the same as that of the magnetic field $\mathbf{H}$ acting on the hydrogel. We further assume that the dipole moment of a mesh element is not influenced by the dipole fields of surrounding mesh elements for low magnetic fields.[41] Thus, the magnetic field experienced by mesh element 1 is given by

$$\mathbf{H}_1 = \mathbf{H}_{ext} \quad (3)$$

where $\mathbf{H}_{ext}$ is the external magnetic field applied. The dipolar interaction energy between mesh elements using the above

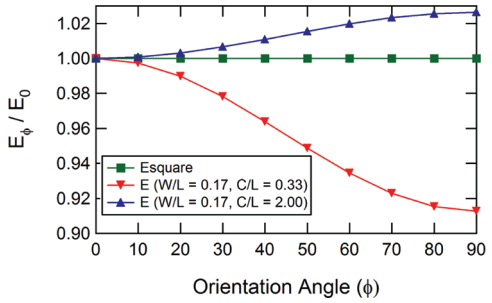

Figure 2. Energy at different orientations, evaluated using FEI, nondimensionalized by the energy in the 0° orientation for three representative shapes. The energy of a square (particle with all sides of equal length) is independent of orientation.

approximations is given by

$$U_{12}(r_{12},\theta_{12}) = \frac{m^2\mu_o}{4\pi}\left(\frac{1-3\cos^2\theta_{12}}{{r_{12}}^3}\right) \quad (4)$$

The energy of a quasi-2D shape of thickness T is given by the sum of the interactions between all the mesh elements in the hydrogel. The nondimensionalized energy obtained using eqs 2 and 4 is given by

$$E_\phi = \frac{U_\phi}{\frac{M^2T^2L\mu_o}{8\pi}} = \kappa^4 \sum_{\Omega}\left\{\left(\frac{x_2-x_1}{L}\right)^2(1-3\sin^2\phi) + \left(\frac{y_2-y_1}{L}\right)^2(1-3\cos^2\phi) - 6\left(\frac{x_2-x_1}{L}\right)\left(\frac{y_2-y_1}{L}\right)\sin\phi\cos\phi\right\} \Bigg/ \left[\left(\frac{x_2-x_1}{L}\right)^2 + \left(\frac{y_2-y_1}{L}\right)^2\right]^{5/2} \quad (5)$$

where (x_1,y_1) and (x_2,y_2) are the centers of the mesh elements and $\kappa = s/L$ is the nondimensionalized mesh size. This formulation was used to determine optimal orientations of the particles under applied magnetic fields using FEI described below and off-lattice Monte Carlo (MC) simulations (see the Supporting Information).

3. FINITE ELEMENT INTEGRATION (FEI)

We use the FEI method to evaluate the energy of an H-shaped particle in different orientations. FEI involves summing the interaction energy between each of the mesh elements as shown in eq 5. We varied ϕ from 0° to 90° and evaluated the energy using FEI for typical H shapes as shown in Figure 2. We found that the minimum energy was at 0° (vertical, looks like an H aligned in the direction of the magnetic field) or 90° (horizontal, looks like an I aligned in the direction of the magnetic field), or that all ϕ were of the same energy (Figure 2). Hence, in our larger sweep of parameter space, we compared the energies in the 0° (E_0) and 90° (E_{90}) orientation to determine the preferred orientation (when $E_0 \neq E_{90}$) or the phase boundary (defined by $E_0 = E_{90}$).

The energy given by eq 5 diverges as $O(1/\kappa)$ in the limit of $\kappa \rightarrow 0$ (compare with rod, Supporting Information), since in a 2D lattice the number of terms in the summation grows as $1/\kappa^2$ (nearest neighbors) and $1/r^3 \sim 1/\kappa^3$. The beads encapsulated in a magnetic hydrogel have a physical volume with a diameter d. Comparing our model with the magnetic hydrogel, d sets a physical minimum for the mesh size and hence rectifies the divergence seen in the model. Furthermore, we use non-Brownian H-shaped particles in our study so that the magnetic energy is the only important energy scale. We showed that the product of the energy with κ converges for two values of W/L and three values of C/L in both the 0° (see the Supporting Information) and 90° orientation. The decrease in the product is less than 10% as we decrease κ from 0.010 to 0.007 (see the Supporting Information). Furthermore, the computation time increases as $1/\kappa^4$. Therefore, for numerical convenience, we elected to use a κ of 0.007 (with a reasonable computation time of ~30 min) to evaluate the energy of an H-shaped particle in any orientation. We demonstrated that the phase boundary is invariant to the choice of κ by varying κ over an order of magnitude from 0.0167 to 0.0017 (see the Supporting Information). The interaction energies between all the mesh elements were summed using MATLAB.

4. EXPERIMENTAL SECTION

4.1. Materials. All particles used in this work were synthesized from 35% poly(ethylene glycol) (700) diacrylate (PEG-DA, Sigma Aldrich), 5% Darocur 1173, and 60% 800 nm magnetic bead suspension (Seradyn Inc., carboxylate-modified, 5% solids).

4.2. Stop Flow Lithography. Photomasks of H shapes with desired geometric lengths were designed using AutoCAD 2005 and printed using a high resolution printer at Fine Line Imaging (Colorado Springs, CO). The mask was inserted into the field stop of the microscope and UV light flashed through it using a Lumen 200 (Prior). A filter set that allowed wide UV excitation (11000v2: UV, Chroma) was used to filter out light of undesired wavelengths. Microfluidic devices, made of PDMS, as described in a previous work,[40] were used for the synthesis of magnetic hydrogels. The devices used were rectangular channels of height 30 μm with two inlets. The width in the inlet and polymerization region of the channels was 50 and 300 μm, respectively. The two streams (see the Supporting Information) were flowed in, and SFL was used to synthesize H-shaped particles of desired size using appropriate photomasks and stop, polymerization, and flow times of 400, 75, and 700 ms respectively. The dimensions of the magnetic hydrogels synthesized are given in Table 1.

4.3. Particle Recovery and Characterization. Each batch consisted of 1000 particles synthesized using SFL, suspended in deionized water with 0.005% (v/v) Tergitol NP-10 (Sigma-Aldrich), and collected in an Eppendorf tube. The particles were washed five times using a vacuum manifold with MultiScreen filter plates (Millipore) with pore diameter of 1.2 μm. The cleaned particles were suspended in 300 μL of solution in an Eppendorf tube and stored for use in rotation experiments. Magnetic hydrogels having a solids loading of 3% (same composition as those used in this work), synthesized using SFL, have been characterized previously using alternating gradient magnetometry (AGM, MicroMag 2900). The AGM magnetization curves for both the Seradyn beads and the magnetic hydrogels have been reported in the Supporting Information of a prior publication by our group.[42] The saturation magnetization and mass susceptibility obtained from the AGM curves are, respectively, 28 emu/g and 0.981 cm^3/g for the beads and 3 emu/g and 0.105 cm^3/g for the magnetic hydrogels.

4.4. Rotation Experiments. Rotation experiments were performed in PDMS reservoirs with length, width, and height of 5 mm each. The reservoirs were made by cutting out square sections of side

Table 1. Summary of All Experiments Carried out at Different Values of W/L and C/L for Particles with $L = 60\ \mu$m[a]

shape	W (μm)	C (μm)	W/L	C/L	no. of particles	equilibrium configuration	FEI prediction
rod	5	0	0.08	0	80	0.29 ± 1.78	0
rod	10	0	0.17	0	74	−0.28 ± 1.30	0
H	10	20	0.17	0.33	68	−0.06 ± 1.10	0
H	10	40	0.17	0.67	53	−0.79 ± 3.58	0
H	10	60	0.17	1	57	−0.25 ± 2.73	0
H	**10**	**100**	**0.17**	**1.67**	**59**	**2.27 ± 55.26**	**90**
H	10	120	0.17	2	58	87.14 ± 7.56	90
H	10	150	0.17	2.5	52	89.62 ± 1.70	90
rod	20	0	0.33	0	59	−0.46 ± 3.28	0
H	20	20	0.33	0.33	59	0.41 ± 3.62	0
H	**20**	**60**	**0.33**	**1**	**54**	**2.45 ± 47.68**	**unresolved**
H	20	100	0.33	1.67	51	89.68 ± 2.62	90
H	**25**	**40**	**0.42**	**0.67**	**60**	**−11.27 ± 53.60**	**unresolved**
square	**30**	**0**	**0.5**	**0**	**102**	**−40.09 ± 21.81**	**unresolved**
H	**30**	**20**	**0.5**	**0.33**	**52**	**−9.84 ± 42.14**	**unresolved**
H	30	60	0.5	1	52	89.64 ± 2.79	90
H	*40*	*20*	*0.67*	*0.33*	*51*	*91.18 ± 2.74*	*90*
rod	45	0	0.75	0	59	89.55 ± 3.28	90

[a] The particles have a thickness of 25 μm. The results presented in bold are unresolved by experimentation, whereas the ones presented in italics are resolved but the deviations from the mean equilibrium angle are statistically significant using a 95% confidence interval. Experimental results are defined as resolved if more than 75% of the particles lie within 1° of the mean predicted by FEI.

5 mm from a 5 mm tall PDMS slab. These structures were placed on a PDMS coated glass slide and then bonded by curing overnight at 60 °C in an oven. A 75 μL volume of solution with particles was introduced into the reservoir from the Eppendorf tubes in which particles were stored after recovery. The number of particles introduced into the reservoir was tuned in order to obtain a surface coverage, $S \sim 1\%$, where S is defined as the ratio of the sum of the cross-sectional areas of the particles to the area of the reservoir. An S value of ~1% is low enough to avoid multibody interactions. The particles were allowed to sediment for 1 min after which the reservoir was placed on a microplate shaker (VWR) at 650 rpm for 20 s to randomize the initial orientation of deposited particles. The reservoir with a random orientation of particles was placed on a microscope, and an initial image was taken using a 5× objective and a digital camera (Nikon, D-200). A uniform horizontal magnetic field of 0.005 T was applied using a custom built electromagnet (see the Supporting Information) for varying amounts of time depending on the particles studied, and final images were obtained. For particles that rotated, the magnetic field was kept switched on until all particles had rotated to an equilibrium orientation, the time for which varied between 5 s and 3 min. For 60 μm squares ($W/L = 0.5$, $C/L = 0$), the magnetic field was kept on for 2 h. For all other cases, the magnetic field was kept on for 30 min. The magnetic field varied by <2% over our imaging area as measured using a Gauss/Teslameter Model FW Bell 5060 from Sypris Test and Measurement. We also did not observe large scale movement of particles toward any wall of the reservoir, confirming the uniformity of the magnetic field.

4.5. Assembly Experiments. Assembly experiments were performed in a PDMS reservoir similar to that used for the rotation experiments. A 75 μL volume of solution with suspended particles was introduced into the reservoir from the Eppendorf tubes in which particles were stored after recovery so as to obtain a surface coverage, $S \sim 4.5-5\%$. The particles were allowed to sediment for 1 min before the reservoir was placed on a microplate shaker (VWR) at 650 rpm for 10 s to randomize the initial orientation of deposited particles. The reservoir was then placed on a microscope, and a uniform horizontal magnetic field of 0.005 T was applied using a custom built electromagnet (see the Supporting Information) for 30 min to obtain the final images for further analysis.

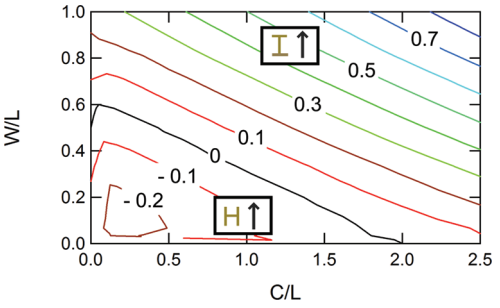

Figure 3. Contour plot for $(E_0 - E_{90})/E_{square}$ as a function of W/L and C/L. The insets show the preferred orientation of the H-shaped particle on applying a uniform magnetic field. The phase boundary is marked by the solid black line. It can be seen that at values of $0.5 < W/L < 0.6$, the preferred orientation changes from 90° to 0° and back to 90°. This preference for the 0° orientation on increasing C/L from 0 up to a certain value of C/L followed by a preference for the 90° orientation on increasing C/L further is seen at all values of W/L.

4.6. Image Analysis. The orientation (angle) of particles with respect to the direction of the magnetic field was found using Image J. The orientation of all the particles in the final image for each of the given values of W/L and C/L shown in Table 1 was recorded, and the deviation of the angles from the equilibrium value predicted using FEI was evaluated.

5. RESULTS AND DISCUSSION

5.1. Rotation Study. H-shaped particles used in this work (Figure 1) can be described by two dimensionless groups: W/L and C/L. A subgroup of particles with $C/L = 0$ constitutes rods of different aspect ratio determined by W/L. Within the rod class is

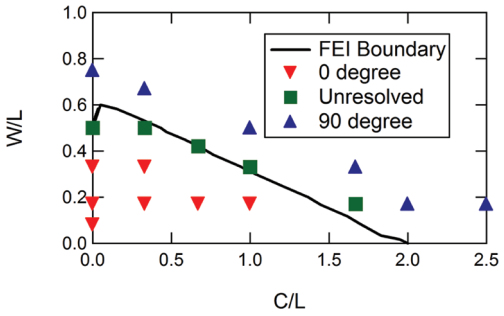

Figure 4. Comparison between experimental results and predictions by FEI. Experimental results are presented using symbols. The solid black line represents the phase boundary predicted using FEI. It can be seen that experimental results are in good agreement with predictions by FEI.

a square which occurs for $W/L = 0.5$. In order to make our calculations independent of the mesh size, we scaled E_0 and E_{90} by the energy of a square particle and plotted the scaled difference to construct the phase diagram shown in Figure 3. The equilibrium orientation of a square-shaped particle is not intuitive. Interestingly, both the FEI technique (Figure 2) and MC simulations (see the Supporting Information) predicted no preferred orientation; that is, all orientations have the same energy. When $W/L \rightarrow 0$, we have two thin vertical rods of equal length connected by a thin horizontal rod. The two orientations for a thin H would have the same energy when the length of the horizontal connector is twice the length of the vertical rods, that is, $C/L = 2$. We cannot use FEI to get predictions for the energies in the two orientations for $W/L = 0$ and $C/L = 2$. However, FEI does predict that in the limit $W/L \rightarrow 0$, the two orientations have the same energy for $C/L \rightarrow 2$. We plotted $W/L = 0$ and $C/L = 2$ as part of the phase boundary as shown in Figure 3.

It can be seen from Figure 3 that the vertical orientation is preferred at low values of W/L and C/L and the horizontal orientation is preferred at higher values of W/L and C/L. For values of $W/L < 0.5$, we observe that, on increasing C/L at a given value of W/L, the preferred orientation changes from the vertical to the horizontal orientation via a phase boundary (shown by the solid black line in Figure 3). At a given value of W/L, on increasing C/L at low values of C/L, $E_0 - E_{90}$ decreases until a certain value of C/L and then increases; that is, the vertical orientation becomes more favored than the horizontal orientation at low values of C/L, followed by the reverse (Figure 3). This phenomenon leads to a re-entrant region at values of $0.5 < W/L < 0.6$, since $W/L = 0.5$ and $C/L = 0$ is a square (has no preferred orientation) and at values of $W/L > 0.5$ and $C/L = 0$, the preferred orientation is horizontal as shown in Figure 3. At values of $W/L > 0.6$, the horizontal orientation is the preferred orientation for all values of C/L, since the initial ($C/L = 0$) difference in energy between the two orientations is too large to be compensated by the initial preferrence for the vertical state on increasing C/L. MC simulations which predict similar trends as FEI (see the Supporting Information) were not able to resolve the re-entrant region in the phase diagram due to the small energy differences between the two orientations. MC simulations also failed to predict an exact phase boundary. However, the phase boundary predicted by FEI lies in the unresolved region predicted by MC simulations (Supporting Information).

Experimentally, we investigated a square particle with side 60 μm, and H shapes with different values of W/L and C/L in the vertical region, horizontal region, and near the phase boundary as shown in Figure 4. We investigated square-shaped particles thoroughly, since both the FEI technique and MC simulations predicted no preferred orientation for these particles. We studied ~100 square particles over 16 sets of experiments, keeping the magnetic field switched on for 2 h in each experiment. We took images at multiple time points (0 min, 30 min, 1 h, and 2 h) and measured the orientation angle at all four times for all particles (see the Supporting Information for one such experiment). The change in orientation from the initial orientation of the particles was statistically insignificant using a 95% confidence interval, at all times. This suggests that square-shaped particles have the same energy in all configurations, validating predictions by the FEI technique and MC simulations.

For H-shaped particles, that is, for values of W/L and C/L shown in Figure 4, we used more than 50 particles to calculate the statistics for reorientation of particles. The mean and standard deviation of the final configurations (after rotation) of the particles for different values of W/L and C/L at which experiments were conducted are reported in Table 1. We observed a distribution of angles as opposed to a single equilibrium orientation for our non-Brownian particles which is most probably due to the friction between the particles and the reservoir bottom. We also calculated the z statistic (assuming a normal distribution) from the mean and standard deviation of the difference between the experimentally observed equilibrium angles and the value predicted by FEI. In most cases, the deviations were not significant using a 95% confidence interval, that is, $-1.96 < z$ statistic < 1.96. The sets of experiments where the deviation was statistically significant have been marked in italics in Table 1. We marked the sets of experiments where we could not resolve (less than 75% of the particles were within 1° of any mean value, i.e., the histograms did not show a clear peak) an equilibrium orientation, in bold in Table 1.

We have shown results from one experiment each at a given value of $W/L = 0.17$ and four different values of $C/L = 0$, 0.33, 1.67, and 2.5 in Figure 5 as an illustrative example, where the preferred orientation changes from vertical to horizontal as C/L increases. Furthermore, at a value of $C/L = 1.67$ (close to the phase boundary), there is no preferred orientation and the magnetic hydrogels do not realign upon switching on the magnetic field. The histograms in Figure 5 show a clear peak around an orientation of 0° for C/L values of 0 and 0.33 and 90° for C/L value of 2.5. However, at a value of $C/L = 1.67$, we see a uniform distribution of orientations from −90° to 90°, within experimental limitations, suggesting no reorientation. The above trend on increasing C/L, that is, preferred vertical orientation, followed by no reorientation, followed by preferred horizontal orientation, was observed for $W/L = 0.33$ as can also be seen in Figure 4.

The experimental results show that there is a region around the phase boundary predicted by FEI wherein the energy difference between the two orientations is too small to be resolved by experiments (Figure 4) and a uniform distribution of angles within experimental limitations instead of a clear peak is obtained. Herein lays the strength of the FEI method as it can predict the equilibrium orientation of H-shaped particles in experimentally unresolvable regions of the phase space. Overall, the experimental results are a good match to predictions by FEI, as shown in Figure 4. Hence, the phase diagram shown in Figure 3 can be used to predict the equilibrium orientation of H-shaped particles of different geometric dimensions.

5.2. Assembly Study. Based on the results of the rotation study, we designed experiments to test the ability of mixtures of

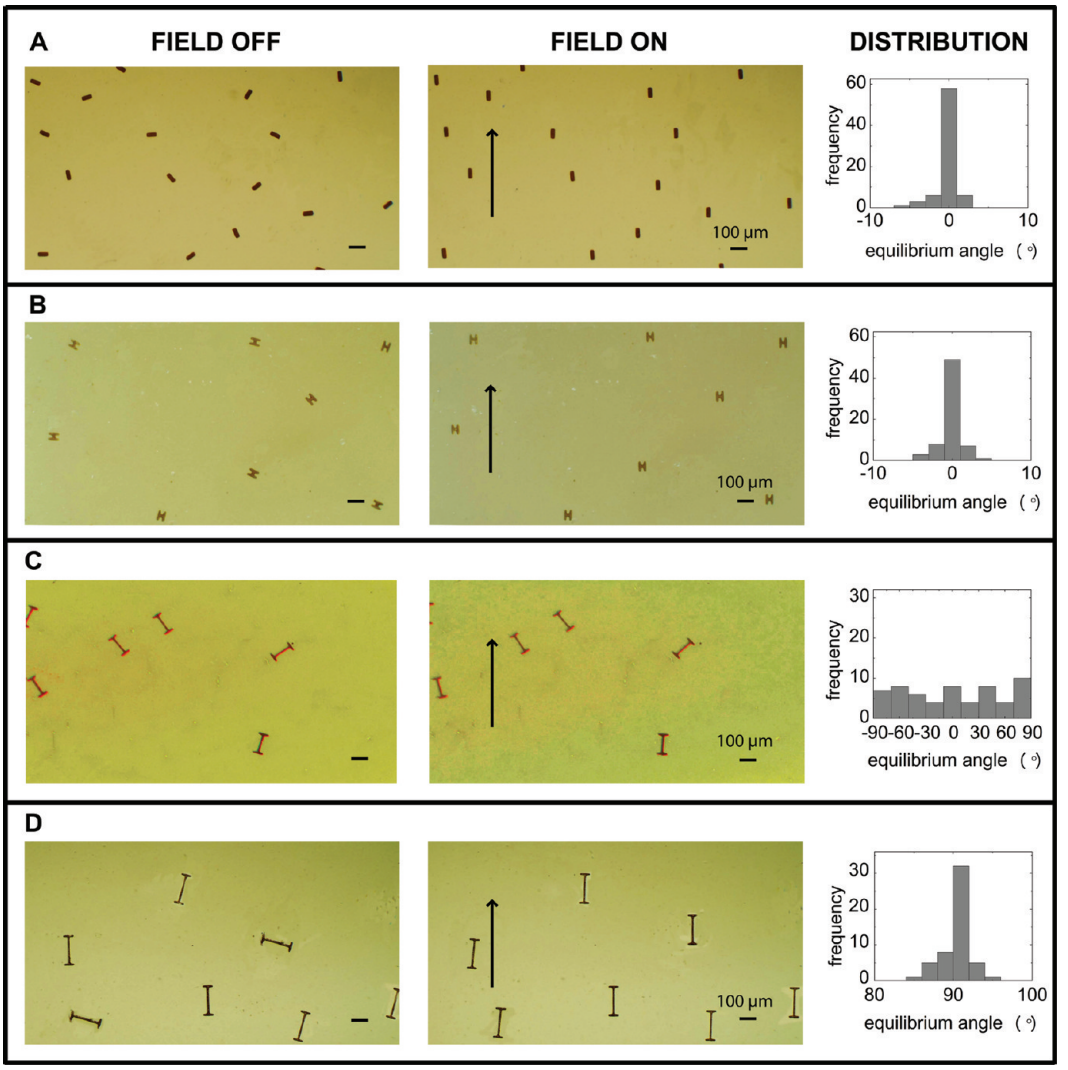

Figure 5. Initial (before switching on the magnetic field of 0.005 T) and final images of magnetic particles with $W/L = 0.17$ and C/L values of (A) 0, (B) 0.33, (C) 1.67, and (D) 2.5. The arrows in the images in (A–D) show the direction of the applied magnetic field. The histograms in (A), (B), and (D) reveal the tight distribution of orientation around 0° for $C/L = 0$ and 0.33 and around 90° for $C/L = 2.5$. For $C/L = 1.67$, there is a uniform distribution of orientations from −90° to 90° within experimental limitations as can be seen in the histogram in (C).

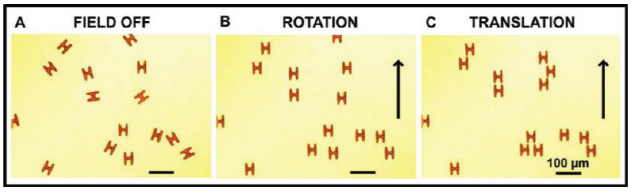

Figure 6. H-shaped magnetic particles (A) before, (B) 1 min after, and (C) 10 min after applying a uniform magnetic field of 0.005 T. The particles first rotate to attain their equilibrium orientation followed by translation to form assembled structures. The arrows show the direction of the applied magnetic field.

rods and H-shaped particles to assemble into wide (orthogonal to the field) chains. In general, the properties of the final assembly of a mixture of rods and H-shaped particles should depend on the total surface coverage of particles (S), the geometric parameters defining the shape, and the fraction of H-shaped particles in the mixture. In this study, we used moderate surface coverage $S = 4.75 \pm 0.25\%$, at which the assembly of anisotropic magnetic particles involves two distinct unrestricted and segmented motions: rotation followed by translation, as shown in Figure 6. Hence, H-shaped particles need to be chosen judiciously so as to orient into desired equilibrium configurations, preceding translation. The H shapes used in the assembly have $C/L = 0.33$ and $W/L = 0.17$ ($T = 25$ μm and $L = 60$ μm). These particles rotate into an equilibrium orientation with the two vertical arms aligned along the magnetic field as shown in Figure 6B. This configuration, as opposed to its orthogonal counterpart, has a higher propensity to induce chain widening and branching during particle assembly. Figure 6C shows the assembled structures formed after translation. The rods used in this work are similar to the vertical arm of an H shape, with $C/L = 0$ and $W/L = 0.08$ ($T = 25$ μm and $L = 60$ μm). In this study, we focus on the effect of varying the fraction of H-shaped particles on the final assembly.

We performed three replicate experiments at three different fractions of H-shaped particles: 0 (only rod-shaped particles), 0.5 (50% mixture of rods and H-shaped particles), and 1 (only

dx.doi.org/10.1021/la2022962 |*Langmuir* 2011, 27, 13428–13435

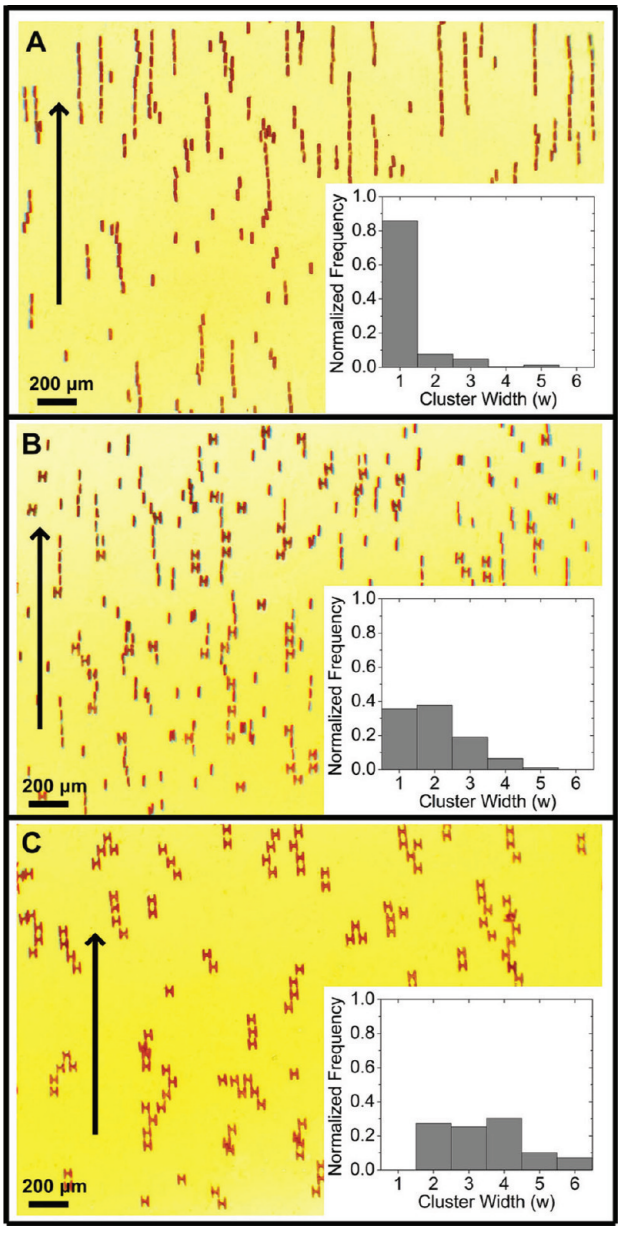

Figure 7. Final assembly images of (A) rods, (B) 50% mixture of rods and H-shaped particles, and (C) H-shaped particles in a uniform magnetic field. The arrows show the direction of the applied magnetic field. The inset plots show the corresponding cluster width histograms. Clusters grow wider with increasing fraction of H-shaped particles.

H-shaped particles). Representative images are shown in Figure 7. We defined the cluster width (w) to be the number of distinct lines parallel to the applied field that can be drawn through a cluster and passing through a rod-shaped particle, or at least through one vertical arm of an H-shaped particle, as depicted in Figure 8. The minimum w for a collection of H-shaped particles is 2. We present the cluster width distribution normalized by the total number of clusters for the three fractions of H-shaped particles in the insets of Figure 7. The cluster width distributions show that clusters widen with increasing fraction of H-shaped particles. In order to investigate whether this widening of clusters could be attributed to differences in the cluster size, we evaluated the site-weighted average cluster

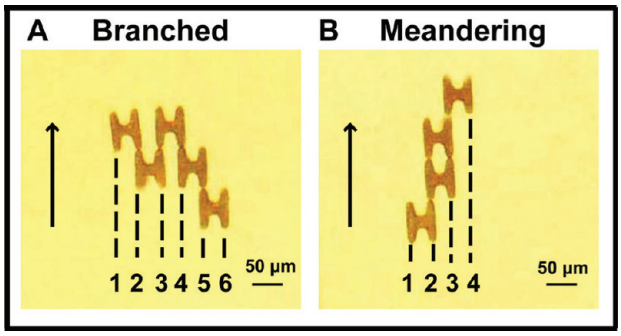

Figure 8. Two different modes of chain growth orthogonal to the applied magnetic field. (A) Branched chain of cluster width 6, formed in this case by two H-shaped particles connecting on the top side of an H-shaped particle and (B) meandering chain of cluster width 4, formed by only one H-shaped particle connecting on one side of an H-shaped particle. The arrows show the direction of the magnetic field.

Table 2. Average Cluster Size (c_{av}), Number of Branching Events (BE), and Branching Events Per Surface Coverage (BE/S_H) of H-Shaped Particles for Different Fractions of H-Shaped Particles Averaged over Three Sets of Experiments for Each Case

H frac	c_{av}	BE	BE/S_H
0	5.9 ± 0.3	4.0 ± 1.0	n.d.
0.5	4.9 ± 0.3	6.3 ± 2.3	2.7 ± 1.0
1	4.6 ± 0.3	10 ± 2.0	2.2 ± 0.5

size[43] using

$$c_{av} = \frac{\sum_{c=1}^{c=\infty} c^2 n(c)}{\sum_{c=1}^{c=\infty} cn(c)} \quad (6)$$

where c is the cluster size and $n(c)$ is the number of clusters of cluster size c. A randomly chosen particle would on average belong to a cluster of size c_{av}. It can be seen from Table 2 that c_{av} is fairly uniform for the three fractions of H-shaped particles used. In fact, c_{av} is highest for a suspension of purely rod-shaped particles and decreases on increasing the fraction of H-shaped particles. Hence, the widening of clusters on increasing the fraction of H-shaped particles cannot be attributed to an increase in c_{av}. The wider cluster size distribution observed on increasing the fraction of H-shaped particles is indeed suggestive of the ability of H-shaped particles to induce chain widening in assembly. Furthermore, a fairly uniform c_{av} combined with a wider cluster size distribution suggests shorter, fatter clusters as opposed to thinner, chainlike clusters.

The widening of chains orthogonal to the field occurs due to the ability of H-shaped particles to connect to other particles on either of their vertical arms. This can happen via two different modes: branching and meandering, as shown in Figure 8. Branched chains are formed when two distinct particles are attached to the vertical arms of an H-shaped particle on the top or on the bottom as shown in Figure 8A. Chain widening in the absence of branching gives rise to meandering structures as shown in Figure 8B. We quantified branching by counting the number of branching events (BE), that is, the number of distinct H-shaped particles attached to two particles either on the top or on

the bottom. For instance, we can observe two BEs in Figure 8A but none in Figure 8B. BE and branching events per surface coverage of H-shaped particles (BE/S_H) for the three fractions of H-shaped particles are reported in Table 2. We see that BE increases on increasing the fraction of H-shaped particles in the mixture, but that BE/S_H is fairly constant, which suggests that part of the chain widening observed on increasing the fraction of H-shaped particles can be attributed to branching.

6. CONCLUSION

In conclusion, we have demonstrated the synthesis of anisotropic H-shaped magnetic hydrogels and the dependence of their equilibrium orientation under an applied magnetic field on geometric shape parameters (W/L and C/L). We developed a framework (finite element integration, FEI) for the theoretical prediction of the equilibrium orientation of H-shaped particles and presented the results in the form of a phase diagram. The predicted phase diagram was validated with experiments. Finally, we demonstrated the ability of H-shaped particles, chosen judiciously from the phase diagram, to induce chain growth orthogonal to the applied field and to form branched structures. FEI can be modified readily to be used for predicting the equilibrium orientation of more complex 2D extruded shapes. Since the assembly of field-responsive particles at low concentrations is a sequential process of rotation followed by translation, the ability to predict the equilibrium orientation of complex 2D extruded particles should be of value in designing particles for assembly. More broadly, we believe that this work will provide a framework to design and investigate microparticles for reverse engineering of target structures through directed assembly.[4,15]

■ ASSOCIATED CONTENT

Supporting Information. Comparison of energy between a 2D extruded and a quasi-2D shape; analysis of a quasi-1D rod; experimental procedure for synthesizing magnetic hydrogels; particle analysis; mesh size dependence of the phase boundary; MC simulations; comparison between MC simulations and FEI technique; convergence for FEI technique; electromagnetic setup. This material is available free of charge via the Internet at http://pubs.acs.org.

■ AUTHOR INFORMATION

Corresponding Author
*E-mail: pdoyle@mit.edu.

■ ACKNOWLEDGMENT

The material is based on work supported by the Singapore-MIT Alliance (SMA-2, CPE Program) and NSF Grant DMR-1006147. The authors thank Dr. D. Trahan and Dr. M. Helgeson for useful discussions. We also thank Murat Ocalan from the Hatsopoulos Microfluidics Laboratory at MIT for the loan of his custom-built electromagnet setup and for useful discussions.

■ REFERENCES

(1) Rabinow, J. *AIEE Trans.* **1948**, *67*, 1308–1315.
(2) Ginder, J. M. *Encycl. Appl. Phys.* **1996**, *16*, 487–503.
(3) Klingenberg, D. J. *AIChE J.* **2001**, *47*, 246–249.
(4) Grzelczak, M.; Vermant, J.; Furst, E. M.; Liz-Marzán, L. M. *ACS Nano* **2010**, *4*, 3591–3605.
(5) Kanu, R. C.; Shaw, M. T. *Int. J. Mod. Phys. B* **1996**, *10*, 2925–2932.
(6) Kanu, R. C.; Shaw, M. T. *J. Rheol.* **1998**, *42*, 657–670.
(7) Watanabe, T.; Aoshima, M.; Satoh, A. *J. Colloid Interface Sci.* **2006**, *302*, 347–355.
(8) Tsuda, K.; Takeda, Y.; Ogura, H.; Otsubo, Y. *Colloids Surf., A* **2007**, *299*, 262–267.
(9) Yin, J.; Zhao, X.; Xia, X.; Xiang, L.; Qiao, Y. *Polymer* **2008**, *49*, 4413–4419.
(10) Bell, R. C.; Miller, E. D.; Karli, J. O.; Vavreck, A. N.; Zimmerman, D. T. *Int. J. Mod. Phys. B* **2007**, *21*, 5018–5025.
(11) Bell, R. C.; Karli, J. O.; Vavreck, A. N.; Zimmerman, D. T.; Ngatu, G. T.; Wereley, N. M. *Smart Mater. Struct.* **2008**, *17*, 015028.
(12) Ngatu, G. T.; Wereley, N. M.; Karli, J. O.; Bell, R. C. *Smart Mater. Struct.* **2008**, *17*, 045022.
(13) de Vicente, J.; Segovia-Gutiérrez, J. P.; A-Reyes, E.; Vereda, F.; H-Álvarez, R. *J. Chem. Phys.* **2009**, *131*, 194902.
(14) de Vicente, J.; Klingenberg, D. J.; H-Álvarez, R. *Soft Matter* **2011**, *7*, 3701–3710.
(15) Glotzer, S. C.; Solomon, M. J. *Nat. Mater.* **2007**, *6*, 557–562.
(16) Ahniyaz, A.; Sakamoto, Y.; Bergstrom, L. *Proc. Natl. Acad. Sci. U.S.A.* **2007**, *104*, 17570–17574.
(17) Lee, S.; Song, Y.; Hosein, I. D.; Liddell, C. M. *J. Mater. Chem.* **2009**, *19*, 350–355.
(18) Ding, T.; Song, K.; Clays, K.; Tung, C. H. *Adv. Mater.* **2009**, *21*, 1936–1940.
(19) Herlihy, K. P.; Nunes, J.; DeSimone, J. M. *Langmuir* **2008**, *24*, 8421–8426.
(20) Isojima, T.; Suh, S. K.; Sande, J. B. V.; Hatton, T. A. *Langmuir* **2009**, *25*, 8292–8298.
(21) Nunes, J.; Herlihy, K. P.; Mair, L.; Superfine, R.; DeSimone, J. M. *Nano Lett.* **2010**, *10*, 1113–1119.
(22) Choi, S. Q.; Jang, S. G.; Pascall, A. J.; Dimitriou, M. D.; Kang, T.; Hawker, C. J.; Squires, T. M. *Adv. Mater.* **2011**, *23*, 2348–2352.
(23) Ge, J.; Hu, Y.; Zhang, T.; Yin, Y. *J. Am. Chem. Soc.* **2007**, *129*, 8974–8975.
(24) Dyab, A. K. F.; Ozmen, M.; Ersoz, M.; Paunov, V. N. *J. Mater. Chem.* **2009**, *19*, 3475–3481.
(25) Yuet, K. P.; Hwang, D. K.; Haghgooie, R.; Doyle, P. S. *Langmuir* **2010**, *26*, 4281–4287.
(26) Gangwal, S.; Cayre, O. J.; Velev, O. D. *Langmuir* **2008**, *24*, 13312–13320.
(27) Gangwal, S.; Pawar, A.; Kretzschmar, I.; Velev, O. D. *Soft Matter* **2010**, *6*, 1413–1418.
(28) Singh, H.; Laibinis, P.; Hatton, T. A. *Langmuir* **2005**, *21*, 11500–11509.
(29) Edwards, B.; Mayer, T. S.; Bhiladvala, R. B. *Nano Lett.* **2006**, *6*, 626–632.
(30) Tierno, P.; Claret, J.; Saguès, F. *Phys. Rev. E* **2009**, *79*, 021501.
(31) Lee, S.; Liddell, C. M. *Small* **2009**, *5*, 1957–1962.
(32) Grzybowski, B.; Whitesides, G. M. *Science* **2002**, *296*, 718–721.
(33) Qi, Y.; Wen, W. *J. Phys. D* **2002**, *35*, 2231–2235.
(34) Teixeira-Pinto, A. A.; Nejelski, L. L.; Cutler, J. L.; Heller, J. H. *Exp. Cell Res.* **1960**, *20*, 548–564.
(35) Saito, M.; Schwan, H. P.; Schwarz, G. *J. Biophys.* **1966**, *6*, 313–327.
(36) Yang, M.; Lim, C. C.; Liao, R.; Zhang, X. *J. Microelectromech. Syst.* **2006**, *15*, 1483–1491.
(37) Blakemore, R. P. *Science* **1975**, *190*, 377–379.
(38) Bazylinski, D. A.; Frankel, R. B. *Nat. Rev. Microbiol.* **2004**, *2*, 217–230.
(39) Shine, A. D.; Armstrong, R. C. *Rheol. Acta* **1987**, *26*, 152–161.
(40) Dendukuri, D.; Gu, S. S.; Pregibon, D. C.; Hatton, T. A.; Doyle, P. S. *Lab Chip* **2007**, *7*, 818–828.
(41) Mohebi, M.; Jamasbi, N.; Liu, J. *Phys. Rev. E* **1996**, *54*, 5407–5413.
(42) Bong, K. W.; Chapin, S. C.; Doyle, P. S. *Langmuir* **2010**, *26*, 8008–8014.
(43) Zallen, R. *The Physics of Amorphous Solids*; John Wiley and Sons, Inc.: New York, 1983.